2D Dion–Jacobson $CsPbI_3$ with Enhanced Interlayer Coupling for Stable and Efficient Photovoltaics

Lei, Yutian; Peng, Guoqiang; Wang, Haoxu; Wang, Gang; Yang, Siwei; Wang, Qian; Li, Zhen Hua; Jin, Zhiwen

DOI
10.1002/admi.202201501

Publication date
2022

Document Version
Final published version

Published in
Advanced Materials Interfaces

ADVANCED MATERIALS INTERFACES
www.advmatinterfaces.de

2D Dion–Jacobson $CsPbI_3$ with Enhanced Interlayer Coupling for Stable and Efficient Photovoltaics

Yutian Lei, Guoqiang Peng, Haoxu Wang, Gang Wang, Siwei Yang, Qian Wang, ZhenHua Li, and Zhiwen Jin**

Inorganic 2D layered $CsPbI_3$ is awaiting to overcome the phase instability of traditional 3D components. However, the most reported Ruddlesden–Popper (RP) phase 2D $CsPbI_3$ leads to larger interlayer distance and weaker interlayer coupling since the existence of the van der Waals gap, which deteriorates the performance of the device and makes the improvement of stability unsatisfactory. Herein, this work resorts ethylenediamine cations (EDA^{2+}) to construct a series of Dion–Jacobson (DJ) phase 2D $CsPbI_3$ as $(EDA)Cs_{n-1}Pb_nI_{3n+1}$ with van der Waals gap eliminated. Combining simulation calculations and experiments, it is found that the $(EDA)Cs_{n-1}Pb_nI_{3n+1}$ has enhanced intermolecular forces to overcome the problem of insufficient crystallization power caused by large steric hindrance in the film assembly process compared to phenethylammonium-based RP phase analogues. In addition, profit from the reduced interlayer distance and stronger coupling, the rigidity of the structure is increased, and the annoying non-radiative recombination caused by structural fluctuations is alleviated. As a result, the 2D layered DJ phase $CsPbI_3$-based solar cells deliver eminent performance than RP phase analogues, especially the 2D $(EDA)(Cs)_4Pb_5I_{16}$ ($n = 5$) device exhibits a record PCE of 10.43% in this work, and significantly enhanced stability.

1. Introduction

Inorganic $CsPbI_3$ perovskite solar cells (PSCs) have attracted widespread attention due to their outstanding photovoltaic performance, and their power conversion efficiency (PCE) had exceeded 20%.[1] However, the unpleasant phase transition problem caused by the inappropriate tolerance factor of $CsPbI_3$ seriously impair the long-term stability of the device. Specifically, due to the small size of Cs^+, it is difficult to maintain structural integrity at room temperature and resulted in spontaneously transforms into a yellow non-perovskite phase.[2,3] In response, remarkable efforts have been invested into the design of a more stable $CsPbI_3$ by implementing various methods, including component engineering, additive engineering, dimensional engineering, etc.[4–6]

Typically, a wise choice for ideal dimensional engineering is introducing suitable organic molecules into the $CsPbI_3$ films to act as steric hindrance, sealing and barrier layers. Hence it can realize the stability as 2D (2D, inorganic layer number, $n \leq 5$) or quasi-2D ($n > 5$) CsPbI3 materials, and meanwhile, possess carrier mobility and exciton separation ability that equivalent to 3D bulk materials.[7–9] Currently, as a primary member of the 2D perovskite family, Ruddlesden–Popper (RP) phase 2D (or quasi-2D) $CsPbI_3$ characterized by large-sized organic cation spacer has shown promising future in solar cells.[10–12] Liao et al. first ingeniously introduced butyl ammonium cation (BA^+) into the perovskite precursor as a raw material to induce the formation of $BA_2CsPb_2I_7$. The $BA_2CsPb_2I_7$ film, which intervenes the crystallization process by steric hindrance, maintains structural stability well under certain humidity and temperature, and the corresponding device obtains a PCE of 4.84%.[13] Later, the aromatic molecule phenethylamine cation (PEA^{2+}) has become the minion in the research of RP phase low-dimensional perovskite attribute to its π–π interaction. With the meticulous deduction of research groups such as Wang and Li et al., the quasi-2D $PEA_2Cs_{n-1}Pb_nX_{3n+1}$ ($n = 40$) PSCs achieved an outstanding efficiency of 16.07%.[14,15]

However, the photovoltaic performance of the 2D $CsPbI_3$ based on the RP prototype is obviously far behind compared with the 3D conformation. Furthermore, although these 2D PSCs outperform their 3D counterparts in terms of stability, it is clear that there is still significant room for further improvement in the stability of PSCs. Substantially, this can be

Y. Lei, G. Peng, Q. Wang, Z. Jin
School of Physical Science and Technology
Lanzhou University
Lanzhou 730000, China
E-mail: jinzw@lzu.edu.cn
H. Wang
Photovoltaic Materials and Devices Group
Delft University of Technology
Mekelweg 4, Delft 2628 CD, The Netherlands
G. Wang
Department of Microelectronic Science and Engineering
School of Physical Science and Technology
Ningbo University
Ningbo 315211, China
S. Yang
Laboratory of Graphene Materials and Applications
State Key Laboratory of Functional Materials for Informatics
Shanghai Institute of Microsystem and Information Technology
Chinese Academy of Sciences
865 Chang Ning Road, Shanghai 200050, China
Z. H. Li
School of Physical Science and Technology & Lanzhou Center for Theoretical Physics & Key Laboratory of Theoretical Physics of Gansu Province
Lanzhou University
Lanzhou 730000, China
E-mail: lizhenhua@lzu.edu.cn

The ORCID identification number(s) for the author(s) of this article can be found under https://doi.org/10.1002/admi.202201501.

DOI: 10.1002/admi.202201501

interpret as: 1) In the lattice of RP system, where the spacer cation can only interact with the $[PbI_6]^{4-}$ octahedron on one side of the inorganic perovskite layers and hence a van der Waals gap exist between adjacent organic cations, which inevitably increases the barriers to charge transport in the organic layer.[16,17] 2) Superficially, the hydrophobic chain seems to defend the perovskite structure from the environmental erosion, but in fact, the van der Waals interaction between the $[PbI_6]^{4-}$ octahedron is too weak to maintain the 2D perovskite structural integrity.[18,19]

Theoretically, the Dion–Jacobson (DJ) phase 2D $CsPbI_3$ with diamine cation as interlayer completely eliminates the van der Waals gap by virtue of the direct action of organic cations and inorganic layer.[20–22] Further, the strong hydrogen bonding between the spacer layer and the adjacent inorganic plate of DJ phase 2D perovskite makes it have a sturdier structure and shorter interlayer distance compared with RP phase analogues, which reduces the potential barrier of charge transport in the organic layer.[23–25] In 2017, Zhao et al. tactfully added a small amount 2D DJ phase component ($(EDA)PbI_4$) into the precursor of $CsPbI_3$, revealing that the α-$CsPbI_3$ could be stabilized by 2D constituent to inhibit the formation of undesirable non-perovskite δ-phase formation.[26] This research has offered a guidance of feasibility exploration for the pure component 2D $CsPbI_3$ PSCs. Fang et al. discovered that $(EDA)Cs_{n-1}Pb_nI_{3n+1}$ has excellent photoelectric properties by density functional theory, but there are few experimental practicality studies.[27] Recently, Hou et al. tried to insert the larger organic cation 1,4-butanediammonium (BDA) into an inorganic cesium-lead mixed halide perovskite slabs (i.e., $(BDA)Cs_{n-1}Pb_n(I_{0.7}Br_{0.3})_{3n+1}$) to clarify the phase evolution mechanism and delivered a PCE up to 9.5%, which further stimulated the extensive curiosity about 2D $CsPbI_3$.[28] In a word, compared with vast number of research on monoammonium system, the layered structure of diammonium-intercalated 2D $CsPbI_3$ perovskite is barely explored.

Here, we present ethylenediamine cation (EDA^{2+}), a diamino organic compound as a divalent spacer cation to prepare 2D $CsPbI_3$. First, theoretical simulations show that the DJ phase has stronger intermolecular forces and interlayer coupling compared with RP analogues. Then, to compared with the RP analogue, DJ phase perovskite with different n values of $(EDA)Cs_{n-1}Pb_nI_{3n+1}$ were prepared, revealing that the strong intermolecular force have positive impact in regulating the crystallization process of the $CsPbI_3$ films. As a result, the layered 2D DJ phase $(EDA)Cs_4Pb_5I_{16}$ (n = 5) PSCs obtained a record stable PCE up to 10.43%.

2. Result and Discussion

Different conformations of organic cations (monoamine/diamine) have a significant impact on the final target due to differences in size and intermolecular forces during the process of inserting into the 3D matrix.[29] Considering this, in order to understand the differences of their constituent units and the overall interlayer spacing when different organic cations were inserted, further the discrepancy of its photoelectric performance, the structure of RP ($(PEA)_2Cs_{n-1}Pb_nI_{3n+1}$) and DJ ($(EDA)Cs_{n-1}Pb_nI_{3n+1}$) phase perovskite ($n$ = 2, 3, 5) were analyzed by simulation.

As shown in **Figure 1**a, structurally, for both EDA^{2+} and PEA^{+}-intercalated 2D $CsPbI_3$, each $-NH^{3+}$ group produces three I—H bonds, two of which bond with terminal I^- ions, and one of which bonds with bridging I^- ion of second nearest neighbored atomic layer. Yet a significant difference is that EDA^{2+} eliminates the van der Waals gap through direct interaction with the octahedron at both ends. Furthermore, the amino group of organic spacer cations intrudes into the octahedral cavity and imposes spatial constraints on the Pb—I equatorial plane of $[PbI_6]^{4-}$ octahedron, resulting in steric hindrance effect (Figure 1b).[30,31] Meanwhile, EDA^{2+} with two amino groups at both ends can directly alternately form hydrogen bonds with the inorganic plate, which has the potential to stabilize the 2D $CsPbI_3$ structure.[27,32] The distance between the H atom of the $-NH_3$ group in the spacer cation and the I atom of the Pb–I plane terminal was also calculated to convince this. In Figure 1c, Compared with the RP phase $CsPbI_3$, the N—H...I distance of the DJ phase $CsPbI_3$ is significantly shorter, which indicates that EDA-based 2D perovskite has a stronger hydrogen bond interaction. The formation of this strong hydrogen bond and the existence of previously discussed steric hindrance have a crucial influence on the crystallization kinetics and stability of the film. (It was discussed in detail below).

Notably, the distance between inorganic plates is crucial in the electronic structure and, in turn, for out-of-plane exciton dissociation and energy transfer for 2D perovskites.[33,34] Figure 1d shows the distance of the axial terminal iodine atoms between two perovskite phase structures with different n values through simulation. Obviously, the DJ phase $CsPbI_3$ has a shorter interlayer distance regardless of the number of layers. These reduced I...I distances indicate a strong dynamical interlayer coupling between the inorganic plates in $(EDA)Cs_{n-1}Pb_nI_{3n+1}$. As discussed below, the optoelectronics of DJ phase $CsPbI_3$ was influenced noticeably by the presence of interlayer electronic coupling. In lead halogen perovskite semiconductor, the distortion of structure has obvious effect on the electrical properties and stability of devices. For example, the positions of conduction band (CBM) and valence band (VBM) correlated to band gap are closely related to Pb-I framework.[35] Moreover, phase transitions can be mitigated by the release of structure distortions when environmental stresses are applied to perovskite lattice. This is because the larger distortion reflects the stronger force between organic cations and inorganic components between the layers, which can hinder the diffusion of water molecules into the lattice and inhibit ion migration under thermal stress conditions.[36,37] Here, we use the Pb—I—Pb (I—Pb—I) bond angle to quantify the degree of structure distortion of the DJ and RP phase 2D $CsPbI_3$ (Figure 1f). The Pb—I—Pb (I—Pb—I) bond angles can be divided into the equatorial along the inorganic layer and axial along the stacking axis. Equatorial Pb—I—Pb (I—Pb—I) bonds should be more relevant to the bandgap. What needs to be emphasized is that the Pb—I—Pb (I—Pb—I) bond angle may not be the only determinant for compounds of different structures. Kanatzidis et al. reported that as the interlayer spacing decreases in the 2D composition, the interaction between the inorganic layers becomes stronger, which may also have a significant impact on the band gap.[38] In addition, axial Pb—I—Pb (I—Pb—I) bonds are likely to influence the excitonic behavior.

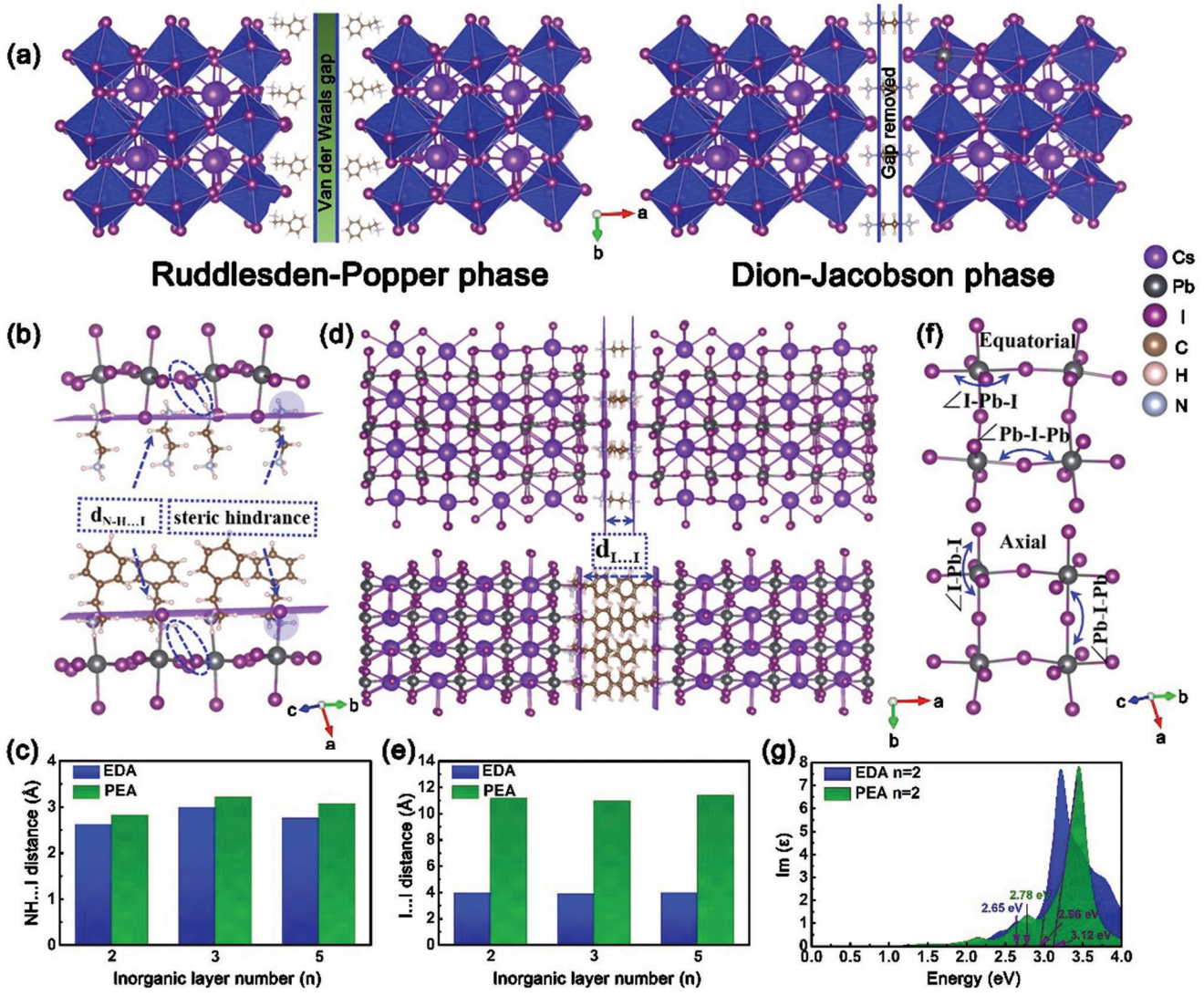

Figure 1. Structural simulation information: a) Schematic illustration of RP and DJ phase 2D layered perovskites; b,c) Hydrogen bond distance comparison of $(EDA)Cs_{n-1}Pb_nX_{3n+1}$ and $(PEA)_2Cs_{n-1}Pb_nX_{3n+1}$, the dash lines indicate the closest NH···I distances; d,e) The structure and data statistics of the interlayer distance defined by the terminal iodide; f) I—Pb—I and Pb—I—Pb angle definition diagrams; g) Two-phase ($n = 2$) exciton effect calculated based on Bethe–Salpeter theory.

As shown Figure S1a, Supporting Information, it is obvious that DJ phase $CsPbI_3$ has smaller Pb—I—Pb equatorial bond angle, indicating that the system has larger adjacent octahedral twist than RP phase analogues, mainly due to the rather strong chemical bonding between the H and terminal I^- anions. Interestingly, the axial Pb—I—Pb bond angle of the former increases with the increase of n value, while the latter remains almost unchanged. When $n = 5$, two kinds of angles are almost the same (Figure S1a, Supporting Information). It can be explained that there is a large interlayer distances in the 2D $CsPbI_3$ of RP phase, and the axial I...I pairs remain spatially apart (>11 Å), so that the effect of electronic coupling along the superposition axis can be ignored, which further proves the strong interlayer coupling in DJ phase $CsPbI_3$. Meanwhile, the I—Pb—I bond angle shows that DJ phase $CsPbI_3$ have smaller $[PbX_6]^{4-}$ octahedral distortion than RP isomorphism (Figure S1b, Supporting Information). This phenomenon could be mainly attributed to the torsion of adjacent octahedral in the strong coupling process that compensates the stress of octahedron preventing the excessive deformation, which has a significant impact on the dissociation of excitons in device operation.[39] Accordingly, the exciton transfer of the two phases was further studied when $n = 2$ based on the Bethe–Salpeter methods (BSE) simulation technology, and the results implied that the DJ phase has a smaller exciton transfer energy (310 meV compared with 340 meV), which reconfirmed the results discussed above (Figure 1g).

Then, DJ phase $CsPbI_3$ films with different number of inorganic layers ($n = 2$, 3, 5, 20, 40, and ∞) were prepared to explore their crystallographic information, optical properties and surface morphology. The change of the number of layers is realized by adjusting the stoichiometric reaction according to the general formula $(EDA)Cs_{n-1}Pb_nI_{3n+1}$. **Figure 2**a shows a simple

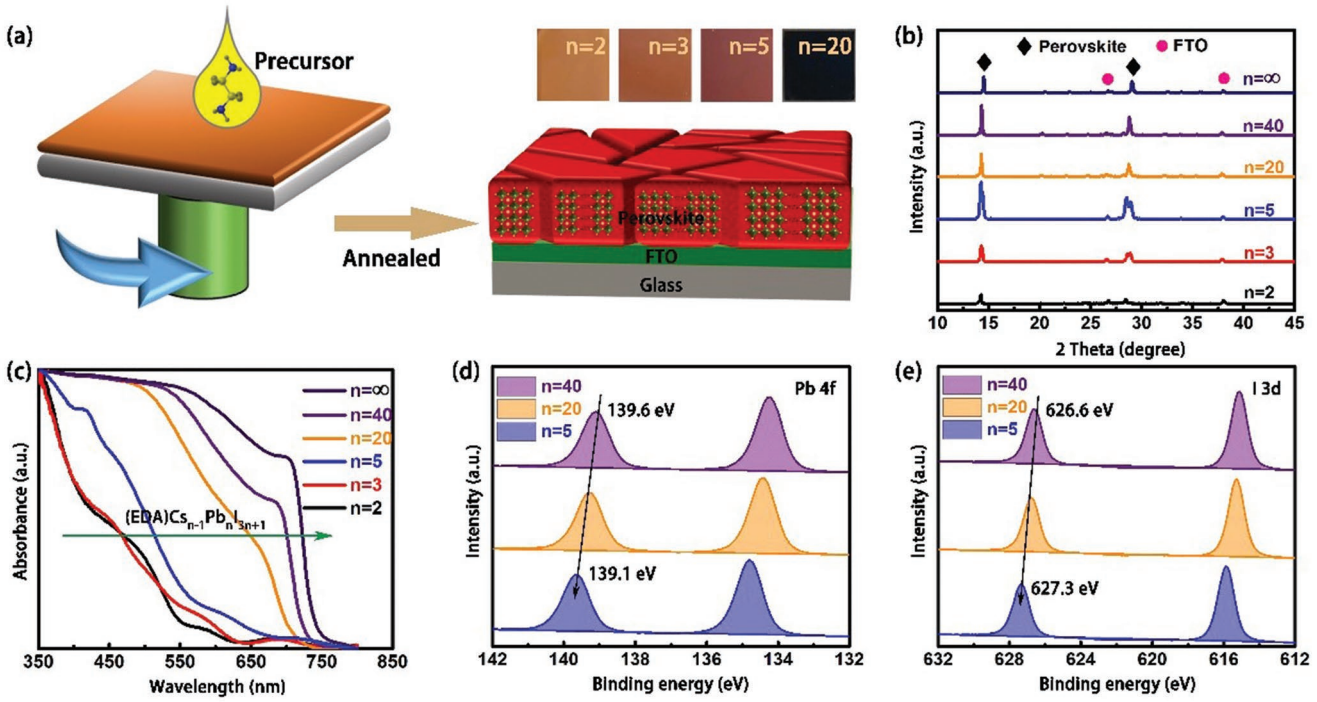

Figure 2. Characterizations of (EDA)$(Cs)_{n-1}Pb_nI_{3n+1}$ films: a) Film preparation process diagram and pictures of different n values; b) XRD patterns for different n numbers; c) UV–vis absorption spectra; d) and e) represent the XPS spectra of Pb 4f and I 3d, respectively.

film preparation process and images of films fabricated with different n-values. Figure 2b shows that all the investigated (EDA)$Cs_{n-1}Pb_nI_{3n+1}$ films have lattice reflections (2θ) around at ≈14° and ≈29°, representing (110) and (100) crystal planes, respectively. Slight shifts of the two peaks toward smaller angles are observed with decreased n values, owing to the lattice expansion caused by organic cations (Figure S2a, Supporting Information). Diffraction peaks split could be observed when n = 3 and 5, which is due to the impure and uneven distribution of the internal phases of the film at low n values, often accompanied by several phases at the same time.[33,40] Subsequently, optical absorption and photoluminescence (PL) spectra were used to study the optical properties of the film. Figure 2c shows that the film emerges continuous redshift and broadening with the increase of the n value; In addition, exciton peaks appear near short wavelengths at low n values (n = 2, 3, and 5). Then it becomes less obvious at high n values because the exciton binding energy decreases with increasing n values.[41,42] Their emission wavelength also appears an obvious red shift with the increase of n value, which is very consistent with the corresponding change of absorption band edge (Figure S2b, Supporting Information). X-ray photoelectron spectroscopy (XPS) was used to study the element information on the surface of the film. Figure 2d,e shows that the Pb 4f and I 3d peaks shift to high binding energy as the value of n decreases, which is due to the strong interaction between EDA^{2+} and Pb—I framework. It is reported that more 3D-like phases with weaker intermolecular forces tend to accumulate on the surface of the quasi-2D perovskite film (n = 20, 40), and this situation is alleviated when the value of n is small.[43,44]

The structural information was further confirmed by scanning electron microscopy (SEM) and atomic force microscopy (AFM). Obvious differences for various n values were found. As expected (**Figure 3**a,b), there are isolated and disordered crystal grains on the surface of the film with n = 2 with very poor surface coverage. A speculation was made and demonstrated below that this is due to the steric hindrance of a large number of organic cations inhibiting the growth of crystal grains. As the value of n increases, nucleation sites increase due to the weakening of steric hindrance and the increase of intermolecular forces, resulting in the aggregation of fine grains and higher surface roughness; when the number of layers is further increased, the presence of trace organic molecules improves the quality of the film, and the film appears compact and flat. To further confirm our inference, the RP phase with n = 5, 20, 40 films were selected as a comparison found that it has poor crystallinity and coverage, which is quite different from the DJ phase $CsPbI_3$ film (Figure S3, supporting Information). After all, the steric hindrance existing in both phases induces difficulty in crystallization. Yet as clarified in the previous calculation, the strong hydrogen bond and interlayer coupling of DJ phase remedy the lack of power in the crystallization process. Contact angle is an important means to characterize the moisture resistance of films. Figure 3c shows that the contact angle of the film from n = 2 to n = ∞ decreases sharply from 85.1° to 37.8° because the hydrophobic organic cations form a hydrophobic barrier on the surface of the DJ phase $CsPbI_3$ film, thereby inhibiting the erosion of water molecules.

DJ phase $CsPbI_3$ with a nominal n = 5 average composition was chose as the active layer for our solar cells with an architecture FTO/TiO_2/2D $CsPbI_3$/Spiro-OMeTAD/Au which was measured under simulated 1-sun illumination. First, the photovoltaic performance of DJ phase $(EDA)Cs_4Pb_5I_{16}$ solar cells (EDA-5)

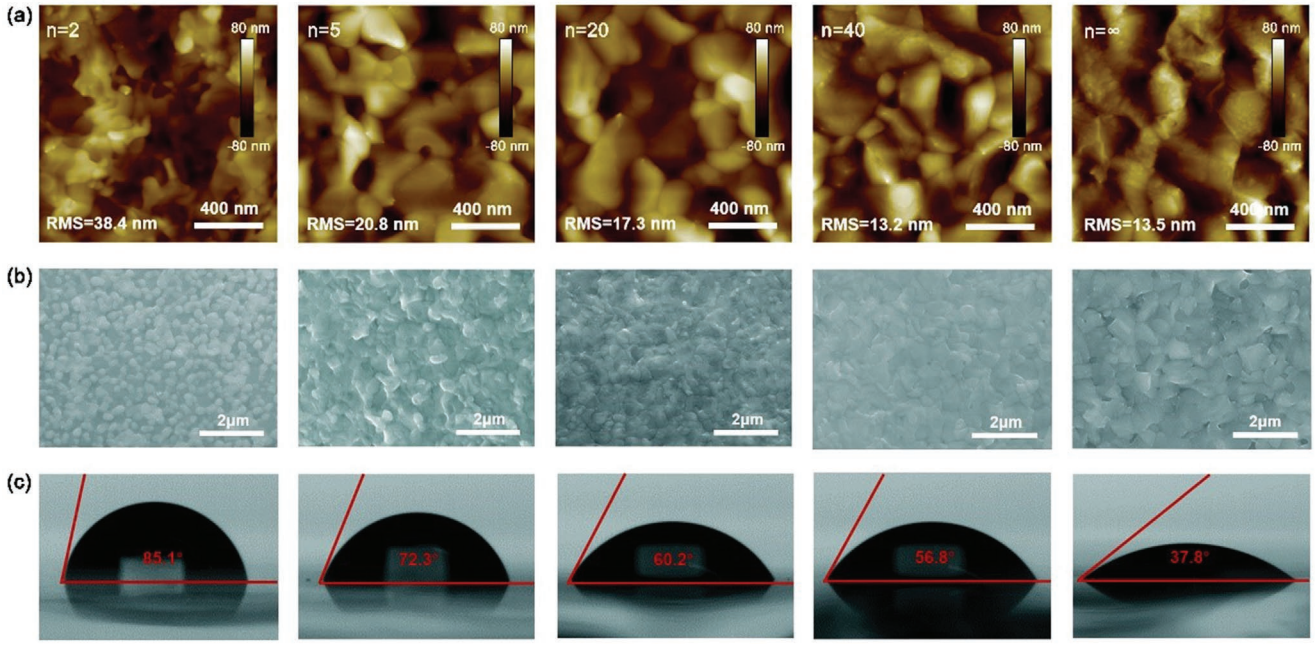

Figure 3. Surface characterization of the (EDA)$(Cs)_{n-1}Pb_nI_{3n+1}$ thin films (n = 2, 5, 20, 40, and ∞): a) AFM, b) SEM, and c) contact angle images.

based on diamine cations was characterized. **Figure 4**a shows the current density–voltage (J–V) curves of the device, and the corresponding parameters are summarized in **Table 1**. This is the highest reported efficiency (10.43%) of inorganic PSCs based on DJ phase $CsPbI_3$ (n = 5). The steady-state power output was measured at a voltage of 0.80 V, and exhibiting a stabilized PCE of 9.2% nearly 1000 s as shown in Figure 4b. The integrated J_{SC} of 12.71 mA cm^{-2} obtained from the external quantum efficiency (EQE) is shown in Figure 4c, which closely matched with the measured J_{SC}. Simultaneously, RP phase $(PEA)_2Cs_4Pb_5I_{16}$

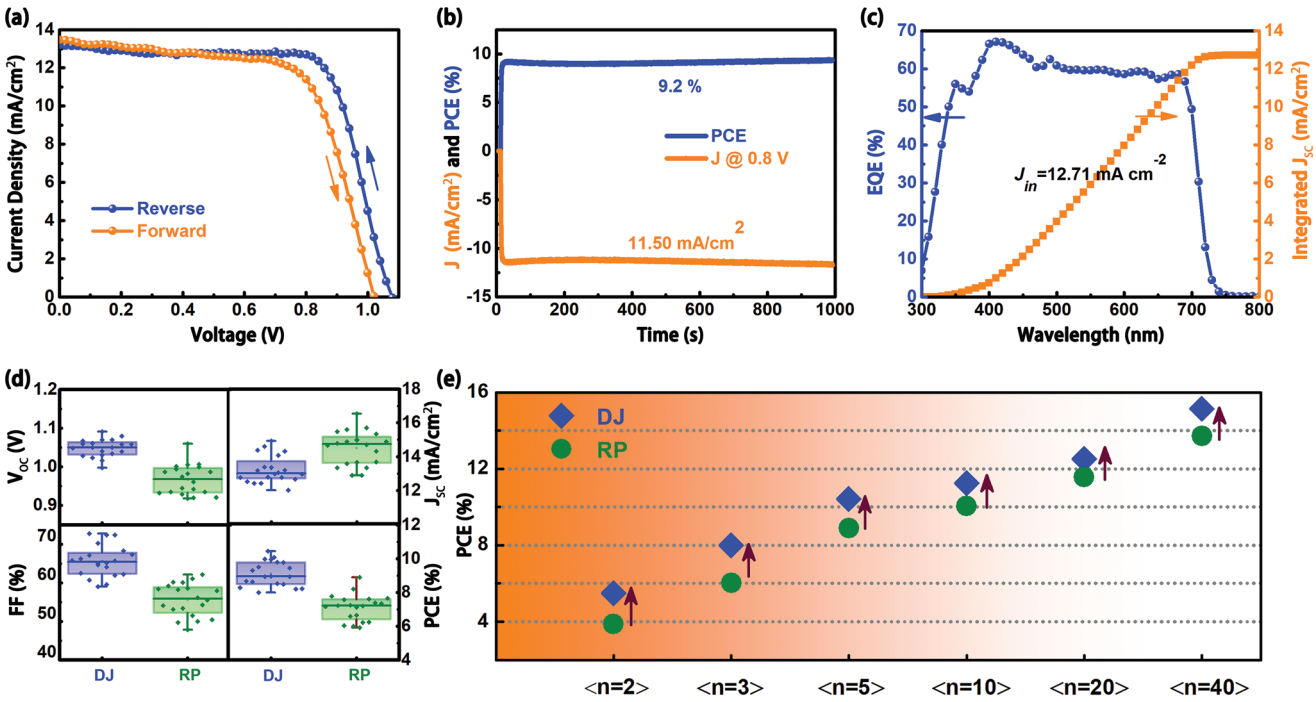

Figure 4. Device performances of the (EDA)$(Cs)_{n-1}Pb_nI_{3n+1}$ and $(PEA)_2(Cs)_{n-1}Pb_nI_{3n+1}$ (n = 5) PSCs: a) J–V curves of the champion PSC; b) Steady measurement at the maximum power output point of 0.80 V; c) EQE and the integrated product of the EQE curve; d) Statistics on the efficiency and other photovoltaic parameters of DJ and RP devices based on 20 samples; e) PCE comparison of the 2D (n = 2, 3, 5), quasi-2D (n = 10, 20, and 40) with RP and DJ phase perovskite.

Table 1. *J–V* parameters of the (EDA)$(Cs)_4Pb_5I_{16}$ device under both forward and reverse scan directions.

Scan mode	V_{OC} [V]	FF [%]	J_{SC} [mA cm^{-2}]	PCE [%]
Forward	1.03	65.33	13.81	9.33
Reverse	1.08	72.37	13.27	10.43

(PEA-5) PSCs were also fabricated under the same conditions, obtaining a PCE of 8.89% (Figure S4a, Supporting Information), lower than that of the EDA-5-based analog. The comparison of specific photovoltaic parameters is shown in Figure 4d, and the efficiency of different values of n is calculated in Figure 4e. It is worth noting that the J_{SC} of the PSC based on PEA-5 is higher than that of the EDA-5. This phenomenon originated from the differences in light absorption ability caused by the different thickness of the active layer, and is mainly induced by the solubility of organic cations in the solvent (Figure S5a,b, Supporting Information).[45,46] In addition, the optical band gap of the DJ phase perovskite is slightly increased compared to RP, which may be caused by the Pb 6p and I 5p orbital overlap changes that induced by the distortion of the Pb—I—Pb structure as mentioned in the previous calculation section (Figure S4d, Supporting Information). Therefore, in the subsequent preparation of high-performance 2D PSCs, attention should be paid to the special structure of organic cations, so as to have higher solvent solubility, facilitate complexation with precursor components, and promote the preparation of thick absorbent layers. At the same time, organic cations with specific functional groups are also expected to regulate the interaction with inorganic layers and reduce the inter-layer charge transport barrier.

In order to explore the underlying reasons for the difference in performance, Mott–Schottky curve was performed to measure voltage loss. As shown in **Figure 5**a, the built-in potential of the PSC based on EDA-5 is 0.94 V, which is higher than that of the PEA-5-based PSC (0.82 V). The larger built-in potential not only enhances the driving force of photogenerated carrier separation, but also an extended depletion region for efficiently suppressing carrier non-radiative recombination at the interface.[47–49] Accordingly, the dark current generated by the carrier recombination at the interface is also identified. Figure 5b shows the dark current density of the two devices, in which EDA-5 is nearly two orders of magnitude smaller than PEA-5, implying fewer recombination, which can be further confirmed by trap state density.[50] As shown in Figure S5a,b, Supporting Information, the bulk defect state density of the film has been deeply insighted by the space charge current limiting (SCLC) method.[18] Deriving from the curve fitting, the corresponding trap density N_t is calculated as 1.23×10^{15} cm^{-3} (2.38×10^{15} cm^{-3}) and 1.30×10^{16} cm^{-3} (1.46×10^{16} cm^{-3}) for EDA-5 and PEA-5 devices in electron-only (hole-only), respectively. We further introduce the time-resolved photoluminescence (TRPL) techniques to exam the quality of the 2D $CsPbI_3$ films, as shown in Figure 5c. The double exponential fitting results show that the RP phase $CsPbI_3$ films decayed with a short lifetime of 2.16 ns compared to DJ samples (13.5 ns), indicating the EDA-5-based samples have less defect state density and extended charge carrier lifetime, which is consistent with the above results.[51,52]

This phenomenon was further demonstrated by studying the dependence of V_{OC} on the change light intensity (Figure 5d).

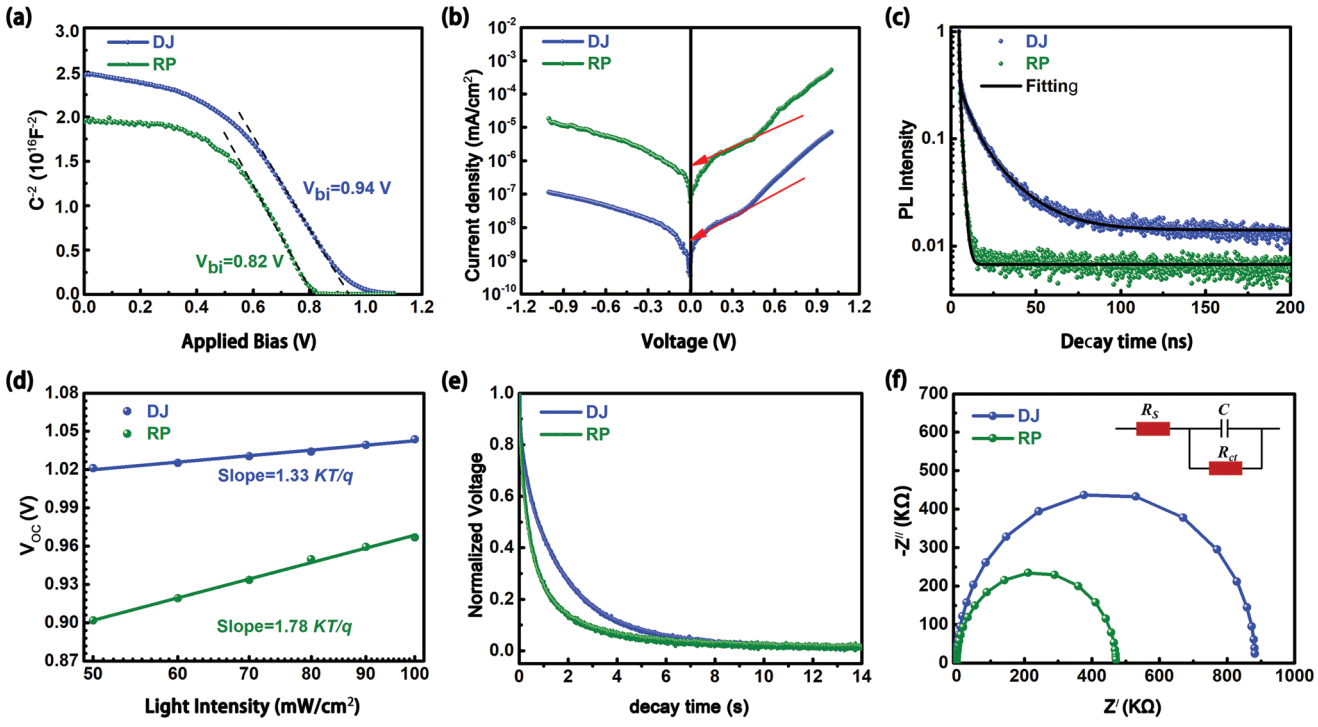

Figure 5. Optoelectronic performances of 2D (EDA)$(Cs)_{n-1}Pb_nI_{3n+1}$ and $(PEA)_2(Cs)_{n-1}Pb_nI_{3n+1}$ (n = 5) devices: a) Mott–Schottky curves; b) dark *J–V* curves; c) TRPL spectra; d) V_{OC} versus light intensity on a seminatural logarithmic scale; e) Open-circuit voltage decay curves; f) Nyquist plots (inset shows the equivalent circuit) of the devices.

The V_{OC} and the corresponding light intensity have a linear relationship on the log scale for both the PEA-5 and EDA-5. The trap-assisted recombination can be well reflected by the deviation between the slope and the value of (kT/q) (k is the Boltzmann constant, T is temperature, and q is the electric charge).[53,54] Decreases in different devices based on EDA-5 and PEA-5 were observed, from 1.33 to 1.78 kT/q, respectively, which suggesting a lower rate of trap-assisted recombination in the former. Similarly, the carrier lifetime of the 2D $CsPbI_3$ PSCs are studied by the transient photovoltage (TPV) decay method, in Figure 5e. The results indicate that the V_{OC} decay with EDA-5 is much slower than that with PEA-5. The lower V_{OC} decay is associated with the longer charge carrier lifetime, which is also in accordance with the lower rate of charge recombination. To analyze the dynamics of charge transfer and recombination in PSCs, the electrical impedance spectroscopy (EIS) was performed. Figure 5f shows the Nyquist plots of devices based on EDA-5 and PEA-5 devices. Specifically, an equivalent circuit consisting of a series charge recombination resistance (R_S), a parallel charge extraction resistance (R_{CT}) and a parallel capacitor (C) is depicted in the inset.[55,56] Clearly, PSCs based on EDA-5 shows large R_s (882 kΩ) than the PEA-5 (471 kΩ), rather, the former has a slightly smaller R_s (108 Ω) than the latter (131 Ω). The high R_c and low R_{tr} for the devices indicated the suppressed carries recombination and enhanced charge transfer, thereby contributing to higher FF value.

Combined with simulation analysis, the differences of photovoltaic performance between RP and DJ phase $CsPbI_3$ origins from the microstructure. In the RP phase $CsPbI_3$, the weak coupling between the inorganic layer and the organic cation greatly enhances the electron-phonon interaction and dominates the non-radiative recombination. In this process, the electron energy of photo-induced carriers is rapidly transferred to the vibrational motion of lattice, which is the main reason for the deterioration of its performance. Compared with RP phase $CsPbI_3$, a single organic cation in DJ phase $CsPbI_3$ eliminates the opportunity of organic barrier generated by intermolecular van der Waals interaction, and reduces the distance between the inorganic layers and enhances the coupling effect. In addition, the stronger interaction between the organic molecule and the inorganic layer enhances the overall lattice strength and thus improves the structural rigidity. Thereby, these special structural characteristics reduce the structural fluctuation of the lattice, weaken the thermally induced electron-phonon coupling and prolong the carrier lifetime.

The phase stability of the film is a prerequisite for the long-term operation of the device. For thermal stability, as shown in **Figure 6**a, the 2D DJ phase $CsPbI_3$ film (n = 5) maintained phase stability under the thermal stress of 65 °C for nearly 600 h, which may be stem from the increase of structural stiffness caused by the enhancement of intermolecular force and interlayer coupling, thus inhibiting the heat-induced ion migration. Correspondingly, the device efficiency maintained nearly 85% after heating for more than 200 h. It is worth noting that the degradation of device performance may also be related to the slow failure of the buffer layer or the electrode. Similarly, under the environmental erosion of ≈40% humidity, the DJ component film remains structurally intact within 72 h, and

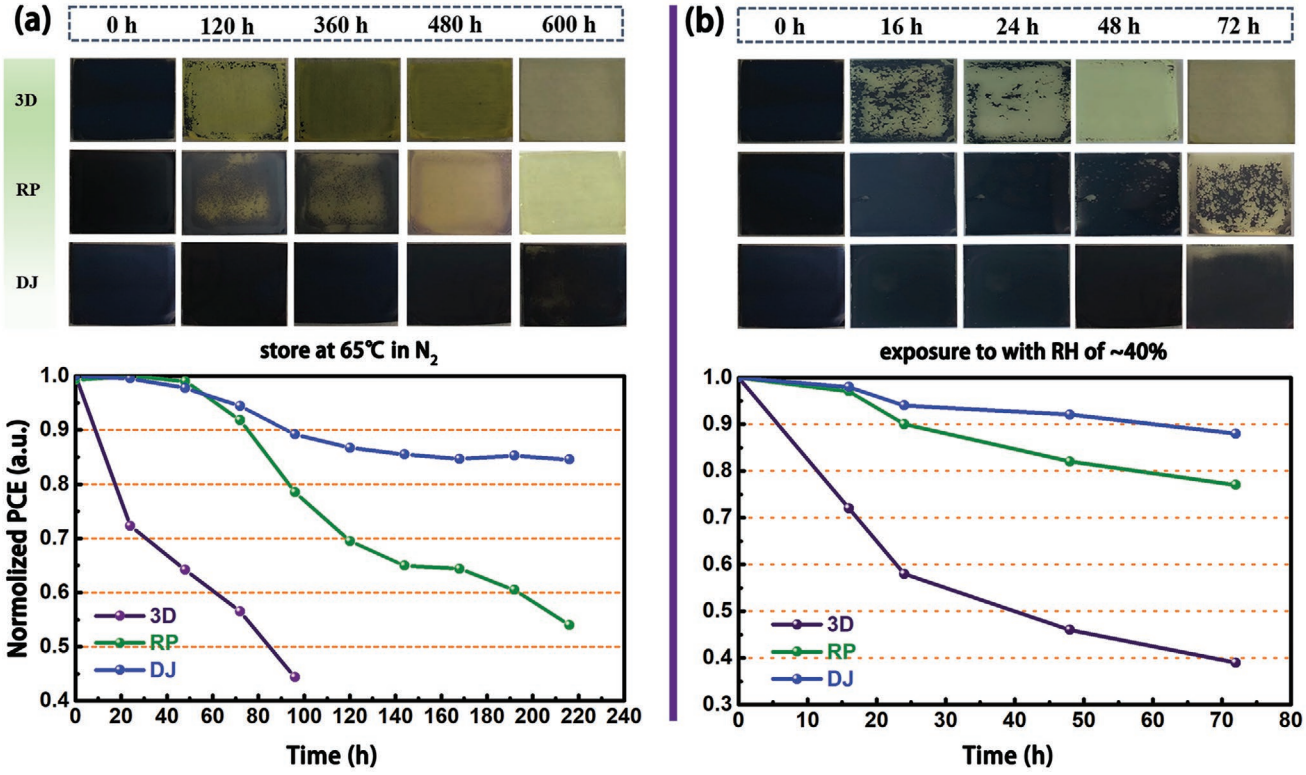

Figure 6. Film and device stability characteristics: Images and the normalized PCEs of the device with $n = \infty$, RP and DJ a) stored at 65 °C in N_2 condition; b) exposed to air with RH of ≈40%.

the corresponding device efficiency also remains above 85%, while the efficiency of RP and 3D phase device decays to 80% and less than 40%, respectively (Figure 6b). This phenomenon is attributed to the hydrophobic organic cations and the improved film morphology, and more importantly, the enhancement of the interlayer interaction inhibits the diffusion of water, oxygen, and other molecules in the structure.[57,58] It is noteworthy that 2D perovskites tend to show more obvious humidity stability in previous reports in the literature. In our study, the low solubility of organic cations limited the protection they could provide from the hydrophobic barrier. In contrast, the above calculations show that the DJ phase has stronger interlayer forces and interlayer coupling, which can largely avoid the destruction of the 2D sufficient by ion migration due to thermal excitation.

3. Conclusion

In conclusion, the subtle interaction between organic components and inorganic perovskite layers in DJ phase results in a smaller interlayer distance, which further leads to stronger coupling and structural strength. This special structure suppresses the quantum confinement effect; bring about efficient charge separation and fast carrier mobilities. As a result, the 2D inorganic (EDA)$Cs_4Pb_5I_{16}$ PSCs achieved a recording efficiency of 10.43%, and the stability of the device in terms of humidity and thermal conditions was greatly improved. In short, although the efficiency of 2D devices with low *n* value still needs to be mentioned, this study clarifies the check and balance relationship between structure and performance, which reminds us that the subtle interaction between organic cations and inorganic frame layers greatly affects the charge carrier dynamics, especially in the design of low-dimensional perovskite photovoltaic devices in the future.

Supporting Information

Supporting Information is available from the Wiley Online Library or from the author.

Acknowledgements

Y.L. and G.P. contributed equally to this work. This work was funded by the National Natural Science Foundation of China (52073131, 51902148, and 12047501), the Fundamental Research Funds for the Central Universities (lzujbky-2020-61, lzujbky-2021-it31, lzujbky-2021-ct15, and lzujbky-2021-ct01). The calculation work was supported by Supercomputing Center of Lanzhou University.

Conflict of Interest

The authors declare no conflict of interest.

Data Availability Statement

The data that support the findings of this study are available from the corresponding author upon reasonable request.

Keywords

2D inorganic perovskite, Dion–Jacobson, efficiency and stability, layer coupling, Ruddlesden–Popper

Received: July 9, 2022
Revised: August 1, 2022
Published online:

[1] NREL, https://www.nrel.gov/pv/device-performance.html (accessed: August 2021).
[2] Z. Li, F. Zhou, Q. Wang, L. Ding, Z. Jin, *Nano Energy* **2020**, *71*, 104634.
[3] J. X. P. Yue, *Front. Phys.* **2021**, *16*, 33204.
[4] D. Bai, J. Zhang, Z. Jin, H. Bian, K. Wang, H. Wang, L. Liang, Q. Wang, S. F. Liu, *ACS Energy Lett.* **2018**, *3*, 970.
[5] J. Zhang, G. Hodes, Z. Jin, S. F. Liu, *Angew. Chem., Int. Ed.* **2019**, *58*, 15596.
[6] Y. Cheng, L. Ding, *SusMat* **2021**, *1*, 324.
[7] Y. Li, H. Cheng, K. Zhao, Z.-S. Wang, *ACS Appl. Mater. Interfaces* **2019**, *11*, 37804.
[8] W. Fu, J. Wang, L. Zuo, K. Gao, F. Liu, D. S. Ginger, A. K. Y. Jen, *ACS Energy Lett.* **2018**, *3*, 2086.
[9] W. Fu, H. Liu, X. Shi, L. Zuo, X. Li, A. K. Y. Jen, *Adv. Funct. Mater.* **2019**, *29*, 1900221.
[10] L. Mao, R. M. Kennard, B. Traore, W. Ke, C. Katan, J. Even, M. L. Chabinyc, C. C. Stoumpos, M. G. Kanatzidis, *Chem* **2019**, *5*, 2593.
[11] J. Hu, I. W. H. Oswald, S. J. Stuard, M. M. Nahid, N. Zhou, O. F. Williams, Z. Guo, L. Yan, H. Hu, Z. Chen, X. Xiao, Y. Lin, Z. Yang, J. Huang, A. M. Moran, H. Ade, J. R. Neilson, W. You, *Nat. Commun.* **2019**, *10*, 1276.
[12] N. Liu, P. Liu, H. Ren, H. Xie, N. Zhou, Y. Gao, Y. Li, H. Zhou, Y. Bai, Q. Chen, *ACS Appl. Mater. Interfaces* **2020**, *12*, 3127.
[13] J.-F. Liao, H.-S. Rao, B.-X. Chen, D.-B. Kuang, C.-Y. Su, *J. Mater. Chem. A* **2017**, *5*, 2066.
[14] K. Wang, Z. Li, F. Zhou, H. Wang, H. Bian, H. Zhang, Q. Wang, Z. Jin, L. Ding, S. Liu, *Adv. Energy Mater.* **2019**, *9*, 1902529.
[15] Z. Li, B. Ma, Y. Xu, Y. Lei, W. Lan, G. Wang, W. Li, Q. Wang, H. L. Zhang, Z. Jin, *Adv. Funct. Mater.* **2021**, *31*, 2106380.
[16] C. Zhao, W. Tian, Q. Sun, Z. Yin, J. Leng, S. Wang, J. Liu, K. Wu, S. Jin, *J. Am. Chem. Soc.* **2020**, *142*, 15091.
[17] T. Niu, Q. Xue, H.-L. Yip, *Nanophotonics* **2021**, *10*, 2069.
[18] Y. Lin, Y. Fang, J. Zhao, Y. Shao, S. J. Stuard, M. M. Nahid, H. Ade, Q. Wang, J. E. Shield, N. Zhou, A. M. Moran, J. Huang, *Nat. Commun.* **2019**, *10*, 1008.
[19] S. Ahmad, P. Fu, S. Yu, Q. Yang, X. Liu, X. Wang, X. Wang, X. Guo, C. Li, *Joule* **2019**, *3*, 794.
[20] S. Yu, Y. Yan, M. Abdellah, T. Pullerits, K. Zheng, Z. Liang, *Small* **2019**, *15*, e1905081.
[21] M. C. Gélvez-Rueda, P. Ahlawat, L. Merten, F. Jahanbakhshi, M. Mladenović, A. Hinderhofer, M. I. Dar, Y. Li, A. Dučinskas, B. Carlsen, W. Tress, A. Ummadisingu, S. M. Zakeeruddin, F. Schreiber, A. Hagfeldt, U. Rothlisberger, F. C. Grozema, J. V. Milić, M. Graetzel, *Adv. Funct. Mater.* **2020**, *30*, 2003428.
[22] S. Li, Z. Liu, Z. Qiao, X. Wang, L. Cheng, Y. Zhai, Q. Xu, Z. Li, K. Meng, G. Chen, *Adv. Funct. Mater.* **2020**, *30*, 2005846.
[23] P. Huang, S. Kazim, M. Wang, S. Ahmad, *ACS Energy Lett.* **2019**, *4*, 2960.
[24] A. Dučinskas, G. Y. Kim, D. Moia, A. Senocrate, Y.-R. Wang, M. A. Hope, A. Mishra, D. J. Kubicki, M. Siczek, W. Bury, T. Schneeberger, L. Emsley, J. V. Milić, J. Maier, M. Grätzel, *ACS Energy Lett.* **2020**, *6*, 337.

[25] L. Cheng, Z. Liu, S. Li, Y. Zhai, X. Wang, Z. Qiao, Q. Xu, K. Meng, Z. Zhu, G. Chen, *Angew. Chem., Int. Ed.* **2020**, *133*, 869.
[26] T. Zhang, M. I. Dar, G. Li, F. Xu, N. Guo, M. Gratzel, Y. Zhao, *Sci. Adv.* **2017**, *3*, e1700841.
[27] Z. Fang, M. Shang, Y. Zheng, T. Zhang, Z. Du, G. Wang, X. Duan, K.-C. Chou, C.-H. Lin, W. Yang, X. Hou, T. Wu, *Mater. Horiz.* **2020**, *7*, 1042.
[28] Z. Zhou, S. Yang, K. Xu, H. W. Qiao, J. Xie, Z. Lin, B. Ge, J. He, M. Chen, J. Zhang, Y. Hou, H. Yang, *J. Phys. Chem. Lett.* **2020**, *11*, 747.
[29] Z. Wang, Q. Wei, X. Liu, L. Liu, X. Tang, J. Guo, S. Ren, G. Xing, D. Zhao, Y. Zheng, *Adv. Funct. Mater.* **2020**, *31*, 2008404.
[30] X. Li, W. Ke, B. Traore, P. Guo, I. Hadar, M. Kepenekian, J. Even, C. Katan, C. C. Stoumpos, R. D. Schaller, M. G. Kanatzidis, *J. Am. Chem. Soc.* **2019**, *141*, 12880.
[31] Z. Fang, X. Hou, Y. Zheng, Z. Yang, K. C. Chou, G. Shao, M. Shang, W. Yang, T. Wu, *Adv. Funct. Mater.* **2021**, *31*, 2102330.
[32] Y. Li, J. V. Milic, A. Ummadisingu, J.-Y. Seo, J.-H. Im, H.-S. Kim, Y. Liu, M. I. Dar, S. M. Zakeeruddin, P. Wang, A. Hagfeldt, M. Gratzel, *Nano Lett.* **2019**, *19*, 150.
[33] C. Ma, D. Shen, T.-W. Ng, M.-F. Lo, C.-S. Lee, *Adv. Mater.* **2018**, *30*, 1800710.
[34] L. Gao, X. Li, B. Traoré, Y. Zhang, J. Fang, Y. Han, J. Even, C. Katan, K. Zhao, S. Liu, M. G. Kanatzidis, *J. Am. Chem. Soc.* **2021**, *143*, 12067.
[35] J.-C. Blancon, J. Even, C. C. Stoumpos, M. G. Kanatzidis, A. D. Mohite, *Nat. Nanotechnol.* **2020**, *15*, 969.
[36] D. Ghosh, D. Acharya, L. Pedesseau, C. Katan, J. Even, S. Tretiak, A. J. Neukirch, *J. Mater. Chem. A* **2020**, *8*, 22009.
[37] E. S. Vasileiadou, B. Wang, I. Spanopoulos, I. Hadar, A. Navrotsky, M. G. Kanatzidis, *J. Am. Chem. Soc.* **2021**, *143*, 2523.
[38] X. Li, J. Hoffman, W. Ke, M. Chen, H. Tsai, W. Nie, A. D. Mohite, M. l. Kepenekian, C. Katan, J. Even, M. R. Wasielewski, C. C. Stoumpos, M. G. Kanatzidis, *J. Am. Chem. Soc.* **2018**, *140*, 12226.
[39] D. Lu, G. Lv, Z. Xu, Y. Dong, X. Ji, Y. Liu, *Chemistry* **2020**, *142*, 11114.
[40] G. Jang, S. Ma, H.-C. Kwon, S. Goh, H. Ban, J. S. Kim, J.-H. Kim, J. Moon, *ACS Energy Lett.* **2020**, *6*, 249.
[41] C. Liu, Z. Fang, J. Sun, Q. Lou, J. Ge, X. Chen, E. Zhou, M.-H. Shang, W. Yang, Z. Ge, *ACS Energy Lett.* **2020**, *5*, 3617.
[42] P. Li, C. Liang, X.-L. Liu, F. Li, Y. Zhang, X.-T. Liu, H. Gu, X. Hu, G. Xing, X. Tao, Y. Song, *Adv. Mater.* **2019**, *31*, 1901966.
[43] Z. Xu, D. Lu, F. Liu, H. Lai, X. Wan, X. Zhang, Y. Liu, Y. Chen, *ACS Nano* **2020**, *14*, 4871.
[44] B. E. Cohen, Y. Li, Q. Meng, L. Etgar, *Nano Lett.* **2019**, *19*, 2588.
[45] Y. Zheng, T. Niu, J. Qiu, L. Chao, B. Li, Y. Yang, Q. Li, C. Lin, X. Gao, C. Zhang, Y. Xia, Y. Chen, W. Huang, *Sol. RRL* **2019**, *3*, 1900090.
[46] M. A. Hope, T. Nakamura, P. Ahlawat, A. Mishra, M. Cordova, F. Jahanbakhshi, M. Mladenovic, R. Runjhun, L. Merten, A. Hinderhofer, B. I. Carlsen, D. J. Kubicki, R. Gershoni-Poranne, T. Schneeberger, L. C. Carbone, Y. Liu, S. M. Zakeeruddin, J. Lewinski, A. Hagfeldt, F. Schreiber, U. Rothlisberger, M. Gratzel, J. V. Milic, L. Emsley, *J. Am. Chem. Soc.* **2021**, *143*, 1529.
[47] H. Sun, Y. Zhou, Y. Xin, K. Deng, L. Meng, J. Xiong, L. Li, *Adv. Funct. Mater.* **2019**, *29*, 1808667.
[48] R. A. Awni, Z. Song, C. Chen, C. Li, C. Wang, M. A. Razooqi, L. Chen, X. Wang, R. J. Ellingson, J. V. Li, Y. Yan, *Joule* **2020**, *4*, 644.
[49] C. Ni, Y. Huang, T. Zeng, D. Chen, H. Chen, M. Wei, A. Johnston, A. H. Proppe, Z. Ning, E. H. Sargent, P. Hu, Z. Yang, *Angew. Chem., Int. Ed.* **2020**, *59*, 13977.
[50] Q. Cao, Y. Li, H. Zhang, J. Yang, J. Han, T. Xu, S. Wang, Z. Wang, B. Gao, J. Zhao, X. Li, X. Ma, S. M. Zakeeruddin, W. E. I. Sha, X. Li, M. Gratzel, *Sci. Adv.* **2021**, *7*, eabg0633.
[51] X. Zhao, T. Liu, A. B. Kaplan, C. Yao, Y.-L. Loo, *Nano Lett.* **2020**, *20*, 8880.
[52] M. Linxing, L. Liang, *Nano Res. Energy* **2022**, *1*, e9120005.
[53] N. Zhou, Y. Shen, L. Li, S. Tan, N. Liu, G. Zheng, Q. Chen, H. Zhou, *J. Am. Chem. Soc.* **2018**, *140*, 459.
[54] L. Zhiqun, Z. Chunyi, Q. Liangti, *Nano Res. Energy* **2022**, *1*, e9120005.
[55] Z. Li, N. Liu, K. Meng, Z. Liu, Y. Hu, Q. Xu, X. Wang, S. Li, L. Cheng, G. Chen, *Nano Lett.* **2019**, *19*, 5237.
[56] Z. Ren, K. Liu, H. Hu, X. Guo, Y. Gao, P. W. K. Fong, Q. Liang, H. Tang, J. Huang, H. Zhang, M. Qin, L. Cui, H. T. Chandran, D. Shen, M.-F. Lo, A. Ng, C. Surya, M. Shao, C.-S. Lee, X. Lu, F. Laquai, Y. Zhu, G. Li, *Light: Sci. Appl.* **2021**, *10*, 239.
[57] H. Wang, Z. Qin, J. Xie, S. Zhao, K. Liu, X. Guo, G. Li, X. Lu, K. Yan, J. Xu, *Small* **2020**, *16*, 2003098.
[58] S. Yu, M. Abdellah, T. Pullerits, K. Zheng, Z. Liang, *Adv. Funct. Mater.* **2021**, *31*, 2104342.

